



PAPER • OPEN ACCESS

Multifunctional electroactive electrospun nanofiber structures from water solution blends of PVA/ODA–MMT and poly(maleic acid-*alt*-acrylic acid): effects of Ag, organoclay, structural rearrangement and NaOH doping factors

To cite this article: Murat imek *et al* 2016 *Adv. Nat. Sci: Nanosci. Nanotechnol.* **7** 025009

View the [article online](#) for updates and enhancements.

Related content

- [Structural, mechanical and electrical properties biopolymer blend nanocomposites derived from poly \(vinyl alcohol\)/cashew gum/magnetite](#)
M T Ramesan, P Jayakrishnan, T K Manojkumar et al.
- [Cellulose nanocrystal-filled poly\(acrylic acid\) nanocomposite fibrous membranes](#)
Ping Lu and You-Lo Hsieh
- [New approaches to the development of hybrid nanocomposites: from structural materials to high-tech applications](#)
V A Gerasin, Evgenii M Antipov, V V Karbushev et al.

Recent citations

- [Recent Advances in the Synthesis of Metal Oxide Nanofibers and Their Environmental Remediation Applications](#)
Kunal Mondal

Multifunctional electroactive electrospun nanofiber structures from water solution blends of PVA/ODA–MMT and poly(maleic acid-*alt*-acrylic acid): effects of Ag, organoclay, structural rearrangement and NaOH doping factors

Murat Şimşek¹, Zakir M O Rzayev² and Ulviya Bunyatova³

¹ Department of Biomedical Engineering, Faculty of Engineering, İnönü University, 44280 Malatya, Turkey

² Institute of Science and Engineering, Division of Nanotechnology and Nanomedicine, Hacettepe University, Beytepe, 06800 Ankara, Turkey

³ Department of Biomedical Engineering, Faculty of Engineering, Baskent University, Baglica Campus, 06810 Ankara, Turkey

E-mail: rzayevzmo@gmail.com

Received 9 March 2016

Accepted for publication 11 April 2016

Published 28 April 2016



CrossMark

Abstract


Novel multifunctional colloidal polymer nanofiber electrolytes were fabricated by green reactive electrospinning nanotechnology from various water solution/dispersed blends of poly (vinyl alcohol-*co*-vinyl acetate) (PVA)/octadecyl amine-montmorillonite (ODA–MMT) as matrix polymer nanocomposite and poly(maleic acid-*alt*-acrylic acid) (poly(MAc-*alt*-AA) and/or its Ag-carrying complex as partner copolymers. Polymer nanofiber electrolytes were characterized using FTIR, XRD, thermal (DSC, TGA–DTG), SEM, and electrical analysis methods. Effects of partner copolymers, organoclay, *in situ* generated silver nanoparticles (AgNPs), and annealing procedure on physical and chemical properties of polymer composite nanofibers were investigated. The electrical properties (resistance, conductivity, activation energy) of nanofibers with/without NaOH doping agent were also evaluated. This work presented a structural rearrangement of nanofiber mats by annealing via decarboxylation of anhydride units with the formation of new conjugated double bond sites onto partner copolymer main chains. It was also found that the semiconductor behaviors of nanofiber structures were essentially improved with increasing temperature and fraction of partner copolymers as well as presence of organoclay and AgNPs in nanofiber composite.

Keywords: nanofiber electrolytes, PVA, alternating copolymer, organoclay, AgNPs

Classification numbers: 5.10, 5.11, 5.16

1. Introduction

Conductive polymers are unique materials in their self-assembled supramacromolecular and conjugated structures as possible substitutes for metallic conductors and

 Original content from this work may be used under the terms of the [Creative Commons Attribution 3.0 licence](https://creativecommons.org/licenses/by/3.0/). Any further distribution of this work must maintain attribution to the author(s) and the title of the work, journal citation and DOI.

semiconductors. Polymer electrolytes with high degree of hydrogen bonding and complexing sites as supramacromolecular systems exhibit excellent electrical conductivity. Noto *et al* [1] briefly discussed the history, role, and applications of electrolyte materials. Many organic and inorganic polymers were widely used in electrochemical processing, gas sensors, high energy density batteries, etc [2, 3]. The conductivity and thermal resistance of solid polymer electrolytes can be enhanced via chemical cross-linking, grafting, graft copolymerization, and various modifications of polymer backbone and side-chains, polymer–polymer interactions and blending with other polymers and using doping agents. Electrical conductivity strongly depends on the number and mobility of charge carriers that can be correlated with chemical composition and morphology of polymer materials (fibers, films, and coatings). Polymer materials contained transition metal ions may facilitate charge transportation either by crosslinking or via hybridization of the s–p and d orbitals [4]. According to the well-known Armand's theory, ionic motion in polymer-salt-complex is not due to charges hopping from site to site, but it is a continuous motion occurring in the amorphous region of the polymeric material [5]. Recently, attention of many researchers has also focused on synthesis of various polymer nanocomposites and nanofiber materials, as well as their metal, metal oxide, clay mineral, graphene and carbon nanotube incorporating compositions as excellent conductive nanomaterials [6–11].

Poly(vinyl alcohol) (PVA) is a semi-crystalline, highly biocompatible, non-toxic, and hydrophilic polymer with good chemical and thermal stability. PVA with functional groups has various usages in preparation of functional polymers because of its easy preparation as a bulk material, films, and fibers [12–16]. Since pristine PVA exhibits poor conductivity as $1.25 \times 10^{-15} \text{ S cm}^{-1}$ [17], several researchers used various functional polymers as partner polymer, organic and inorganic doping agents to increase conductivity of matrix PVA based composite materials, especially its nanofiber composites (NFCs) [17–21]. Although PVA forms excellent nanofibers via electrospinning, its applications are limited due to its high solubility in aqueous media. Therefore, PVA fibers have been modified by either chemical [22–24] or physical [25] cross-linking to improve their mechanical properties and water resistance. Park *et al* [23] reported the effects of the degree of hydrolysis on the morphology and diameter of PVA fibers and also explored the water resistance of electrospun PVA/poly(acrylic acid) (PAA) composite fibers cross-linked via heat treatment.

The synthesis and characterization of poly(maleic acid-*alt*-acrylic acid), poly(MAc-*alt*-AA), and its transition metal (Ni^{2+} , Cu^{2+} and Cd^{2+}) complex polyelectrolytes, as well as their temperature dependence of the conductivity behaviors in water solutions and in solid states were a subject of our previous investigations [26, 27]. In this work multifunctional colloidal electrospun nanofiber polyelectrolytes were fabricated from water solution blends of PVA/octadecylamine montmorillonite (ODA–MMT) nanocomposite as matrix polymer and poly(MAc-*alt*-AA) having regularly repeated hydrogen bonded three COOH groups in the form of

deprotonated carboxylate ions and its Ag-carrying complex as partner polymers/copolymers. The effects of partner polymers, the reactive organoclay and structural factors such as physical and chemical *in situ* interfacial interactions via hydrogen bonding and cross-linking, and structural rearrangement via thermal decarboxylation on matrix/partner nanofibers as multifunctional nanofiber electrolytes were investigated. Another aspect of the study was to evaluate the electrical properties of solid state NFCs as colloidal fiber structures in the presence/absence of NaOH as doping agent and before/after thermal treatment.

2. Experimental

2.1. Materials

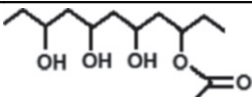
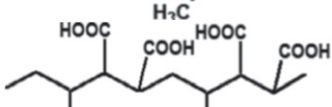
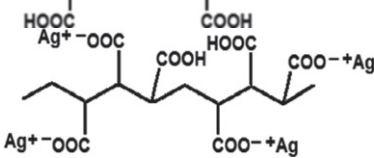
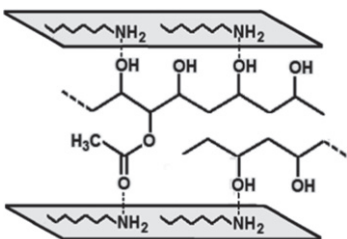
Poly[(vinyl alcohol)_{0.89}-*co*-(vinyl acetate)_{0.11}] (PVA, 89% hydrolyzed, average $M_w = 31.000\text{--}51.000$ Da), octadecyl amine-montmorillonite (ODA–MMT, nanomer I.30E, nanocor Co.) with the following average parameters: content of ODA surfactant-intercalant 25%–30%, particle size 8–10 μm , bulk density 0.41 g cm^{-3} and crystallinity 52.8%, and silver nitrate (AgNO_3 , 99.995%, melting point 202°C with decomposition, $d = 4.35 \text{ g cm}^{-3}$) were purchased from Sigma-Aldrich. Poly(maleic acid-*alt*-acrylic acid) [poly(MAc-*alt*-AA)] with content of maleic acid unit = 47.17 mass%, glass-transition temperature (T_g) 62.5°C and melting temperature (T_m) 137.5°C , intrinsic viscosity (η_{im}) 1.25 dL g^{-1} in dioxane at 25°C , acid number $878 \text{ mg KOH g}^{-1}$ (by alkali titration), and electrical conductivity (σ) $= 4.06 \times 10^{-12} \text{ S cm}^{-1}$ (by Keithley 6512 electrometer) was synthesized by complex-radical copolymerization method. All other solvents and reagents were analytical grade and used without purification.

The compositions, chemical structures and important assignments of these materials are given in table 1.

2.2. Synthetic procedures

Poly(MAc-*alt*-AA) was synthesized by complex-radical copolymerization according to our previous published method [22]. Briefly, copolymerization of maleic anhydride with acrylic acid at 1:1 molar ratio was carried out in 1, 4-dioxane solution in the presence of benzoyl peroxide (0.1%) as an initiator at 70°C under nitrogen flow. The copolymer was purified by twice precipitating from dioxane solution with n-hexane and washed with several portions of benzene and diethyl ether, and dried under vacuum at 50°C to constant weight. This copolymer was easily dissolved in pure water with hydrolysis of anhydride unit and fully transferred to acid unit with regularly repeated structure as poly(maleic acid-*alt*-acrylic acid). Each unit contained three carboxyl groups with strong intra- and intermacromolecular hydrogen bonding. Water solutions of poly(MAc-*alt*-AA) and its silver carrying complex were used in reactive electrospinning nanotechnology as partner copolymers.

Table 1. The compositions chemical structures and assignments of the materials used in electrospinning.

Materials composition	Chemical structure	Assignments
PVA		Reactive matrix polymer
Poly(maleic acid- <i>alt</i> -acrylic acid) 40 and 20 mass %		Reactive alternating partner copolymer-1
Ag-carrying poly((maleic acid- <i>alt</i> -acrylic acid) 40 and 20 mass %		Ag complex of reactive alternating partner copolymer-2
ODA-MMT clay 5.0 mass %	CH ₃ -(CH ₂) ₁₇ -NH ₂ -MMT	Reactive organoclay-nanofiller
Silver nitrate	AgNO ₃	Precursor for <i>in situ</i> generation of Ag nanoparticles onto nanofibers
Intercalated PVA/ODA-MMT nanocomposite 60 and 80 mass%		Matrix intercalated nanocomposite

2.3. Fabrication procedure of NFCs by electrospinning

Nanofibers from matrix/partner composites were prepared from blends of water dispersion of PVA/ODA–MMT as matrix polymer composite, water solutions of poly(MAc-*alt*-AA) and its Ag-carrying composition as partner polymers by electrospinning method using the following optimized parameters: concentration of polymer solutions of 9% w/v, high voltage of 24 kV, flow rate of 0.5 mL h⁻¹, and distance of 15–20 cm between the tip of the needle and the grounded collector. The prepared polymer solutions were put into a syringe and positive electrode of a high voltage power supply was mounted to needle of syringe whereas its negative electrode was attached on the collector. Then, high voltage was applied to polymer solution blends between needle and collector via syringe pump providing a constant flow rate. Randomly oriented nanofibers were obtained by collecting the fiber webs onto an aluminum foil fixed on stationary collector.

2.4. Characterization and analysis methods

Fourier transform infrared (FTIR) spectra were recorded on a FTIR Nicolet 510 spectrometer in the range of 4000–400 cm⁻¹ with a resolution of 4 cm⁻¹. X-ray powder diffraction (XRD) patterns were performed with a PANANALYTICAL x-ray diffractometer equipped with a CuK α tube and Ni filter ($\lambda = 1.5406 \text{ \AA}$). XRD diffractograms were measured at 2θ angles in the range 1°–70°.

Surface morphology of nanofibers was examined using a scanning electron microscope (SEM, Zeiss Supra). All

specimens were freeze-dried and coated with a thin layer of platinum before testing. Thermogravimetric (TGA) and differential scanning calorimetric (DSC) analyses were performed at linear heating rate of 10 °C min⁻¹ under nitrogen flow using EXTRAR600 TG-DTA6300 and diamond DSC Perkin Elmer thermal analyzers. The thermal degradation temperature taking into account was the temperature at onset ($T_{d(\text{onset})}$) and the temperature of maximum weight loss ($T_{d(\text{max})}$). Electrical conductivity and thermal resistance of nanofiber samples as solid/colloidal electrolytes were measured by using a test chamber (JANIS VPF 100 kryostat). Current through thin fiber film was recorded with a Keithley 2400 current–voltage measurement system. Square-shaped samples (0.25 cm²) with four contact points at the corners were prepared to carry out conductivity measurements which were done according to the van der Pauw method. Experiments were conducted in temperature range of 20 °C–50 °C with 1 °C steps (Keithley 6487 Picoammeter/Voltage source) and pressure range of 50–800 torr. Sample temperature was monitored regularly by using a Pt 100 sensor close to the sample and measured with Lakeshore model 331-temperature controller with sensitivity of ± 0 °C. All measurements were performed with a PC through a GPIB converter card.

3. Results and discussion

3.1. Synthetic pathways and structural rearrangements

The schematic representation of the formation of multi-functional nanofiber structures during electrospinning

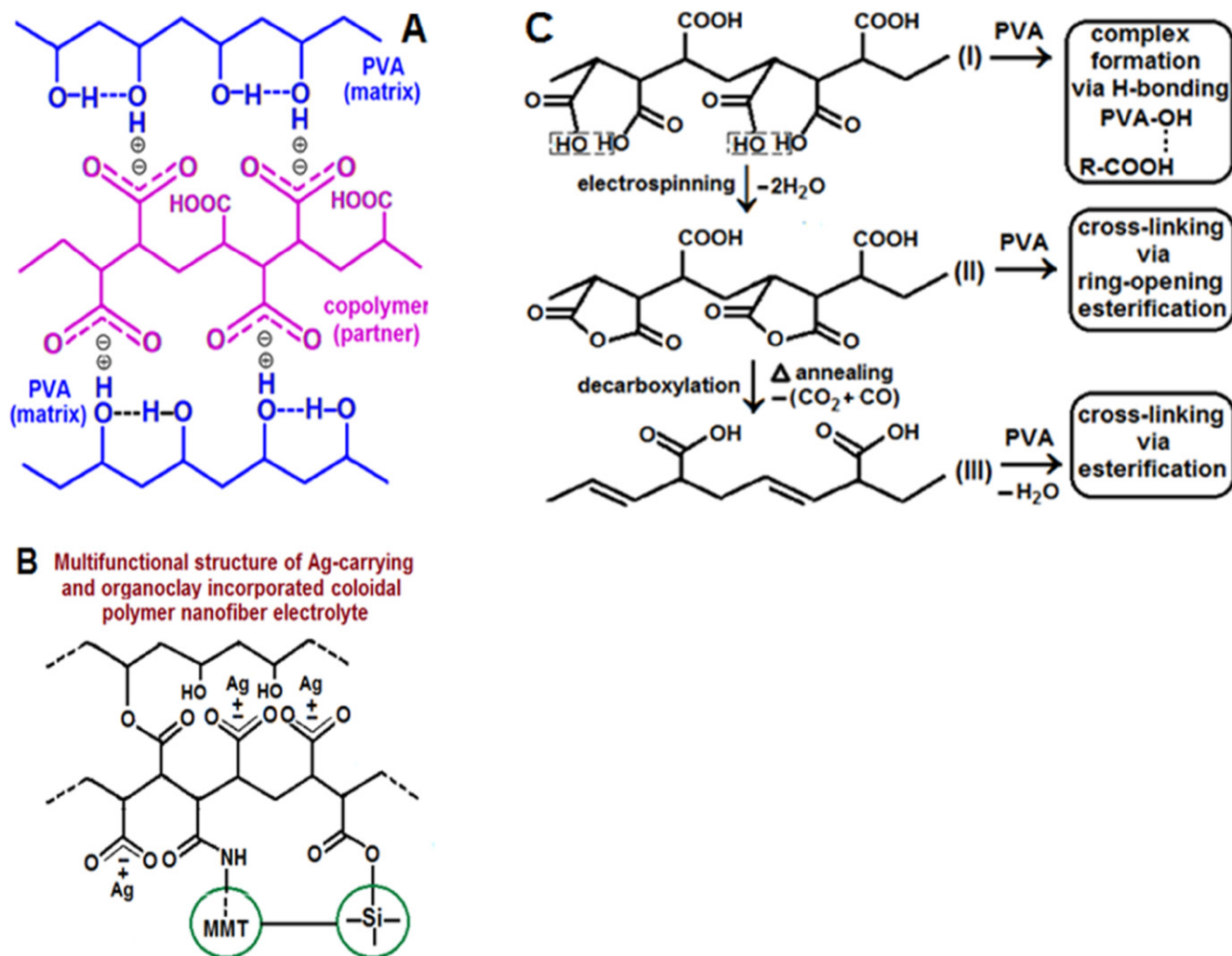


Figure 1. Synthetic pathways and chemistries of multifunctional nanofiber electrolytes: the structure of (A) PVA/poly(MAc-*alt*-AA) complex in water solution, (B) its Ag and ODA–MMT incorporating nanofiber complex and (C) chemical structure changes before and after thermal treatment.

processing is given in figure 1. It was proposed that the following chemical and physical interfacial interactions occurred between PVA and the copolymer (figure 1(A)), the copolymer and ODA–MMT, the copolymer and Ag precursors and *in situ* generated AgNPs (figure 1(B)): (i) esterification/cross-linking of carboxyl groups of the copolymer with hydroxyl groups of PVA which accompanied with release of H₂O molecules (figures 1(A) and (C)); (ii) amidization of carboxyl groups with octadecyl amine intercalant, (iii) esterification/grafting carboxyl groups with ≡Si–OH at edges of MMT clay, and (iv) the formation of Ag-carrying polymer complexes and transformation of Ag precursors to reduced and stabilized AgNPs form onto nanofiber surface during electrospinning (figure 1(B)). In the presented study, thermal treatment were also applied to nanofibers at 25 °C–250 °C with heating rate of 10 °C min⁻¹ in nitrogen atmosphere under vacuum in order to evaluate changes in physical and chemical structure of NFCs. After annealing (figure 1(C)), rearranged structures were formed via decarboxylation of maleic acid units with a release of carbon dioxide (CO₂) and monoxide (CO) [28], and degrading release of acrylic monomer from

copolymer chains [29]. The specific degradation mechanism of homo- and copolymers of maleic anhydride (MA) was also reported by our group [30, 31] and other researchers [32, 33]. Alternating copolymers of MA and their hydrolyzed derivatives exhibit specific thermal degradations which accompanied by the various structural rearrangements at temperature range around 120 °C–500 °C. The degradation mechanism of alternating copolymers of MA with vinyl acetate [34], isopropenyl acetate [35], allyl acetate [36], styrene [37], α-olefins [38] and trans-stilbene [39] were also investigated by many researchers in detail. According to these investigations, thermal decompositions occurred due to the elimination of volatile CO₂ and CO and lead the formation of regular structures with backbone double bonds conjugated to the C=O groups. It was suggested that the structural rearrangements of nanofiber structures can be play an important role in improving conductivity of nanofiber electrolytes due to enhancement of a combination of ion charged sites with chain conjugated double bonds. Thus, the formation of new double bond conjugated sites onto backbone chains is very important factor for enhancement main properties of nanofibers,

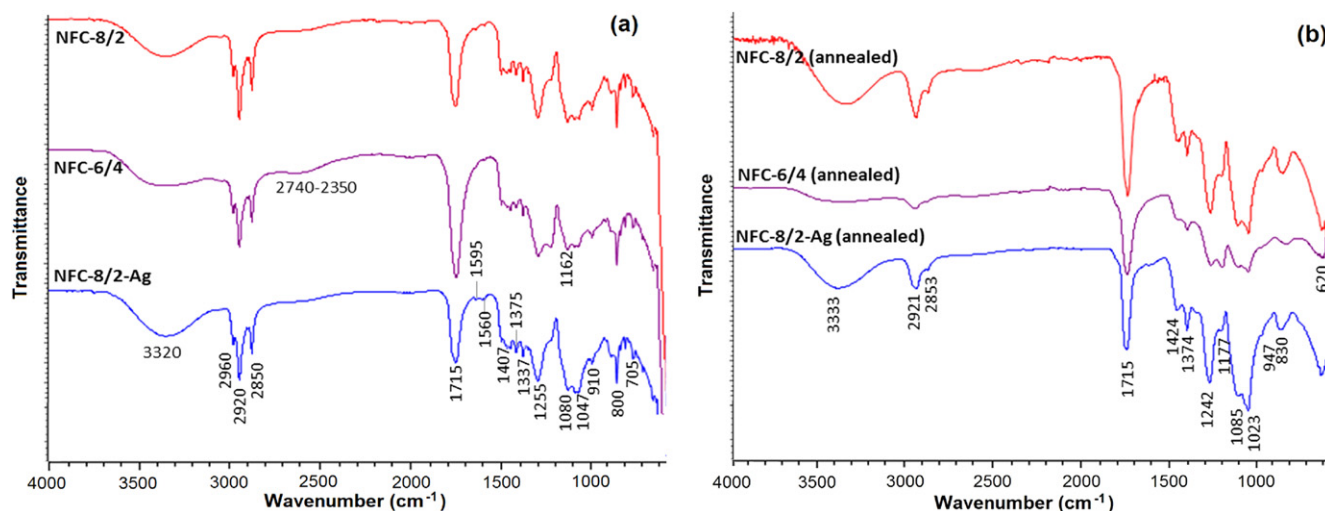


Figure 2. FTIR spectra of NFCs. (a) Before and (b) after annealing.

especially their electrical and thermal behaviors. A new approach reported for the first time in the study can be used in developing polymer nanofiber electrolytes.

3.2. Chemical structures

The chemical structures of NFCs before (figure 2(a)) and after annealing (figure 2(b)) confirmed essentially structural changes indicating the formation of new absorption bands from rearranged fiber structures. FTIR spectra of fiber structures showed the following characteristic absorption bands (figure 2(a)): very broad peak at 3320 cm^{-1} associated with $-\text{OH}$ stretching from strong hydrogen bonding matrix PVA and the partner copolymer through physical interactions of hydroxyl and carboxyl groups. This peak significantly shifted to lower absorption region as compared with absorption band at 3438 cm^{-1} [40] from free non-hydrogen bonding OH group, which is absent in spectra of nanofibers. Three absorption bands at 2960 , 2920 and 2850 cm^{-1} were related to $\text{C}-\text{H}$ stretching in CH_3 , CH_2 and CH groups from backbone chains of the matrix and partner polymers and octadecyl amine group of ODA-MMT. The presence of these groups was confirmed by the antisymmetric deformation bands at 1375 and 1337 cm^{-1} and CH_2 rocking band at 705 cm^{-1} in $-(\text{CH}_2)_n-$ chain. The broad band around $2740\text{--}2350\text{ cm}^{-1}$ can be attributed to $\text{NH}_3^+ -\text{OOC}-$ octadecyl amine/carboxyl hydrogen bonding complex in amine hydrohalides [41].

The bands at 1560 and 1407 cm^{-1} associated with antisymmetric stretching $-\text{COO}-$ in Ag-carrying polymer complexes. Strong fairly band at 1715 cm^{-1} can be attributed to symmetric $\text{C}=\text{O}$ stretching from $-\text{COOH}$ and $-\text{COOR}$ (saturated ester) groups. The intensity of this peak significantly increased with increasing the partner copolymer fraction (NFC-6/4) due to enhancement of the fiber composite with carboxylic and ester groups. This absorption band indicated the occurrence of covalence cross-linking in the nanofibers via esterification of the carboxyl groups of the copolymer with the hydroxyl groups of PVA during electrospinning. Absorption band at 1255 cm^{-1} was related to $\text{C}-\text{O}$

$-\text{C}$ antisymmetric stretching from ester links. The peaks at 1162 and 1047 cm^{-1} can be attributed to $-\text{C}-\text{OH}$ stretching and $-\text{C}-\text{O}-\text{OH}$ secondary alcohol, respectively. The $\text{Si}-\text{O}-\text{Si}$ band from organoclay appeared at 1080 cm^{-1} . The peak at 910 cm^{-1} was related to $\text{C}-\text{O}-\text{H}$ deformation.

FTIR spectra of annealed NFCs are given in figure 2(b). Comparative analysis of the samples before and after annealing indicated the following changes (appearance of new absorption bands, disappearance some bands, and decreases in peak intensities) which conformed the structural rearrangement via predominantly decarboxylation of anhydride units: (i) new peaks at 947 cm^{-1} (backbone chain conjugated $-\text{CH}=\text{CH}-$ band [41]), around 830 cm^{-1} and 620 cm^{-1} ; (ii) almost disappearance of broad band at $2740\text{--}2350\text{ cm}^{-1}$ and strong peak at 910 cm^{-1} , significant decrease in intensity or disappearance of $\text{C}-\text{H}$ stretching in CH and CH_2 groups; (iii) decreases in intensities, especially those in NFC-6/4, and shift of 3320 cm^{-1} broad band to more high region (3333 cm^{-1}). These structural rearrangements which were related to primarily changes of backbone chain and side functional groups ($-\text{OH}$ and $-\text{COOH}$) logically conformed with the above mentioned proposal which is schematically represented in figure 1.

3.3. Physical structures

XRD results which belong to the physical structures of NFCs are given in figure 3. NFC-8/2 and NFC-6/4 having visible weak crystalline peaks at clay region predominantly exhibited amorphous structures (figures 3(a) and (b)), which indicated the transfer of fiber structures to almost fully colloidal state after partially elimination of water molecules during electrospinning via dispersing, absorption and *in situ* physical and chemical processing in the matrix and the partner (copolymer) systems. The characteristic strong reflection peak of neat PVA around 2θ of $19^\circ\text{--}21^\circ$ angles [42] significantly decreased and shifted to the organoclay region. The nanofiber composite incorporated with silver nanoparticles (NFC-8/2-AgNPs) showed higher crystallinity and had more numbers of peak

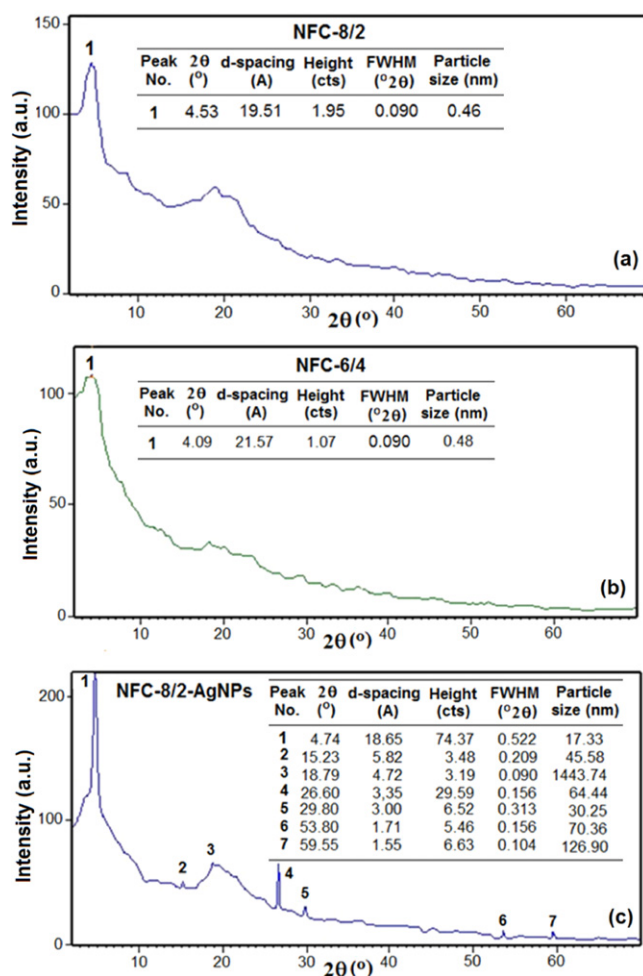


Figure 3. XRD patterns and reflection parameters of NFCs. (a) NFC-8/2, (b) NFC-6/4 and (c) NFC-8/2-Ag. Effect of loading partner copolymer and *in situ* generated silver nanoparticles.

reflections at different angles due to physical interaction of AgNPs with carboxylate ions from the partner polymer (figure 3(c)). The formation of microparticles (1443.74 nm) at angle 2θ of 18.79° can be attributed to the water absorption of colloidal PVA. Observed peaks at angles 2θ of 29.80° and 53.80° can be attributed to the (111) and (200) planes [43] of *in situ* generated AgNPs with sizes of 30.25 and 70.36 nm onto nanofiber surfaces, respectively. It was proposed that the formation of the polymer nanofibers with colloidal amorphous structures during electrospinning of the water dispersed/solution blends of PVA/ODA–MMT and the alternating copolymer not only enhanced with carboxylate ions and their silver complexes, but also *in situ* generated of AgNPs would be take place an important role to improve the electrical properties (conductivity and resistance) of novel kinds of polymer nanofiber electrolytes.

3.4. Surface morphology and fiber diameter distribution of NFCs

Figure 4 presents morphologies and diameter distributions of NFCs with or without the partner polymer. According to the images, all samples exhibited fine fiber morphology. Whereas

PVA/ODA–MMT has average diameter of 276 nm (figure 4(a)), NFC-8/2 and NFC-6/4 exhibit relatively lower average diameter (201 nm and 206 nm, respectively) (figures 4(b) and (c)). This observed fact indicated that the alternating partner copolymer with regular hydrogen bonding carboxylate ions in side-chain essentially influenced the phase separation processing via *in situ* chemical and physical interfacial interactions during electrospinning. It was observed that the morphology, fiber diameters, and diameter distributions strongly depended on the fraction of the alternating partner copolymer in NFC blends which contains regular repeated functional units and their strong hydrogen bonded links via partner–COOH...OH–matrix polymer chains and partner–COOH...NH₂–R (from organoclay). Polymer-copolymer physical interactions easily transferred to covalence bonded structures through esterification and amidation in the phase separation processing during electrospinning.

SEM analysis results of NFC-8/2 (annealed) and NFC-6/4 (annealed) after thermal treatment through chemical structural rearrangements via decarboxylation of maleic anhydride/acid units to form new conjugated double bond sites onto backbone chains of partner copolymer are given in figure 5. This structural phenomenon was confirmed by FTIR and thermal degradation analysis results given in figures 2 and 6, respectively, as well as schematically represented structural rearrangements in figure 1. Morphology parameters such as degree of cross-section density, fiber diameters, and diameter distributions essentially improved due to the effects of these rearrangements after annealing process.

3.5. Thermal behaviors of NFCs

TGA and DTG thermograms of NFCs before and after annealing are given in figure 6. Chemical changes and degradations occurred at increasing temperature conditions. According to the TGA–DTG curves, all NFCs exhibited multi-step degradations via decarboxylation of carboxyl/anhydride units at a temperature range 75°C – 145°C (exothermic peaks). Step infection point (SIP) around 179.20°C – 197.85°C with lower areas for NFC-8/2 and NFC-6/4 was related to release of absorbed water molecules, CO₂ and CO from fiber composites. Intensity of this degradation peaks (doublet) increased in NFC-8/2–Ag sample due to transfer of silver salts to AgNPs. This *in situ* generated AgNPs significantly stabilized the following chain degradation which conformed to almost disappearance of broad peak at $\sim 435^\circ\text{C}$. Two broadening peaks with the higher areas in NFC-8/2 and NFC-6/4 (figures 6(A) and (C)) were associated with the chain degradations of the partner copolymer.

For the full decarboxylation of both maleic and acrylic units it is necessary 38.91 mol% of released products (9.57 mol% H₂O, 26.02 mol% CO₂ and 14.50% CO) which was theoretically calculated as 100% degree of chemical degradative arrangement of the structure in backbone chains of alternating partner copolymer. It was experimentally found that the weight loss values for NFC-8/2 (5.82%), NFC-8/2–Ag (8.90%) and NFC-6/4 (15.71%) corresponded to the

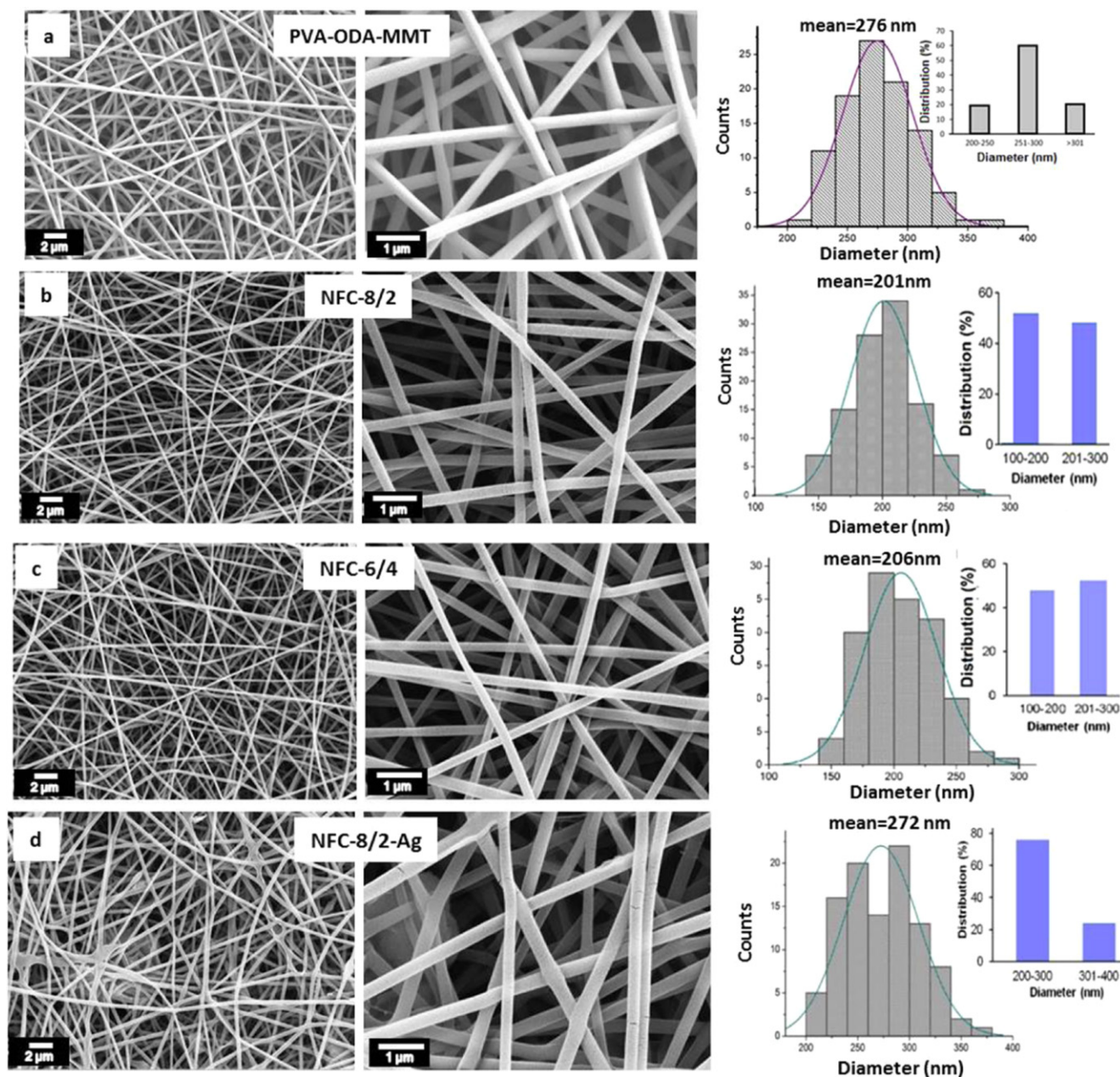


Figure 4. SEM images and diameter distribution of NFCs. (a) PVA/ODA-MMT, (b) NFC-8/2, (c) NFC-6/4 and (d) NFC-8/2-Ag.

decarboxylation degree of 10.94 mol%, 16.74 mol% and 29.55 mol%, respectively. Agreeing with these data, partially degradative rearrangement (structure II in figure 1(C)) occurred during electrospinning process. The above mentioned mechanism of chemical degradative rearrangement was confirmed by fully disappearance of the described endothermic peaks after the annealing process (figures 6(D)–(F)). The results estimated was also logically consistent with the changes of the structural factors observed in FTIR and SEM.

3.6. Electrical properties of NFCs

Figure 7 shows the temperature dependence of conductivity and Arrhenius plot, and TGA–DTG and DSC curves of

pristine alternating copolymer. TGA–DTG analyses showed multi-step degradations for the copolymer (figure 7(a)): via anhydridation of $-\text{COOH}$ groups with release of water molecules at $50\text{ }^{\circ}\text{C}$ – $100\text{ }^{\circ}\text{C}$ (1st step), decarboxylation of anhydride units with elimination of carbon mono- and dioxides at $110\text{ }^{\circ}\text{C}$ – $220\text{ }^{\circ}\text{C}$ (2nd step), and main chain degradations around $240\text{ }^{\circ}\text{C}$ – $300\text{ }^{\circ}\text{C}$ (3rd step) and $390\text{ }^{\circ}\text{C}$ – $450\text{ }^{\circ}\text{C}$ (4th step). DSC curve indicated that the alternating copolymer exhibited glass-transition (T_g) at $62.5\text{ }^{\circ}\text{C}$ and melting (T_m) at $137.5\text{ }^{\circ}\text{C}$. The conductivity of the copolymer underwent a breaking or rearrangement due to increasing temperature (figure 7(b)). In fact, different temperature regions with different activation energies were involved. Above transition temperature, the conductivity of the copolymer increased so

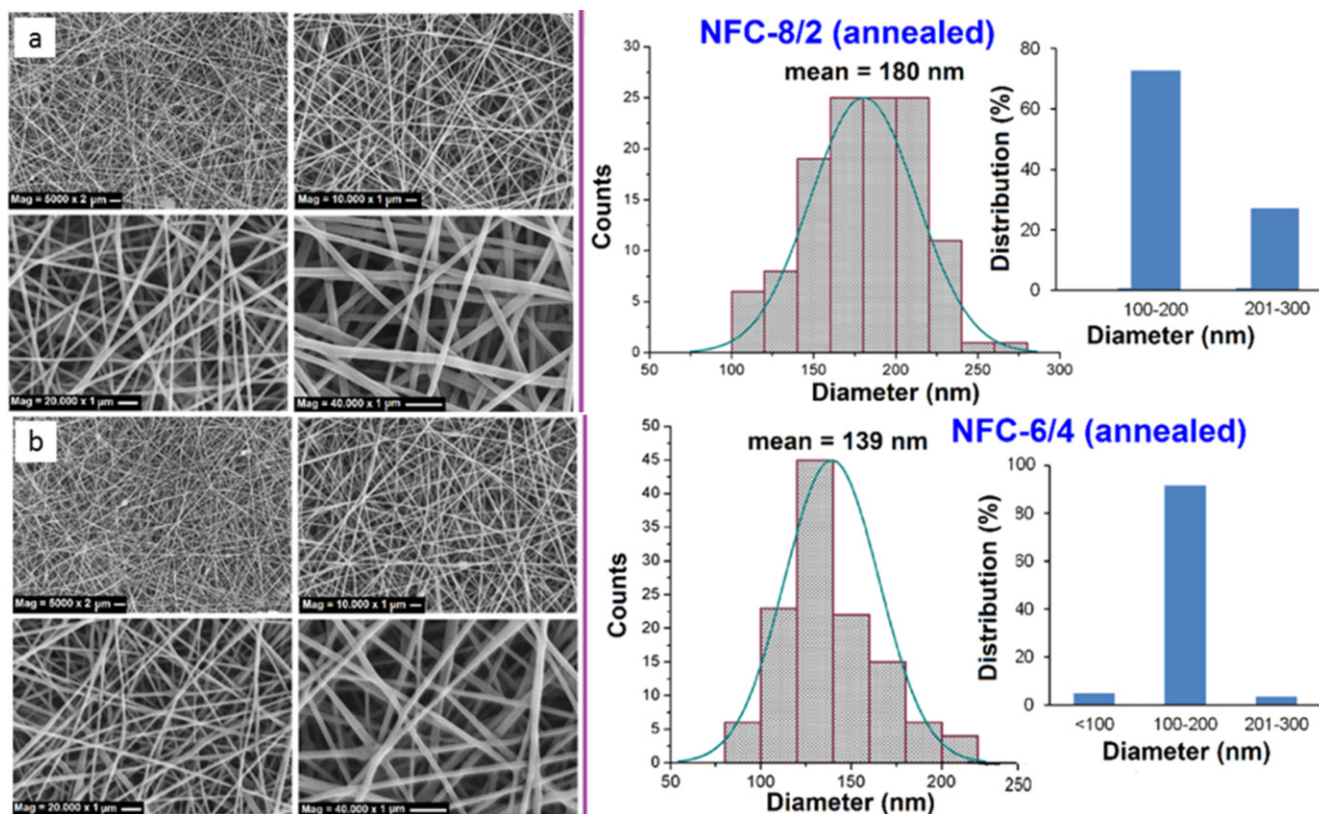


Figure 5. SEM images and diameter distribution of thermal structural rearranged nanofiber composites. (a) NFC-8/2 (annealed) and (b) NFC-6/4 (annealed).

quickly that the activation energy ($E_a = 1.52$ eV) could almost be defined at lower temperature range from 27 °C to 45 °C (figure 7(c)).

Current (I) versus voltage (V) plots at temperature range of 23 °C–70 °C were used to determine the thermal resistance and conductivity values of NFCs (figures 8(A)–(C)). Thermal resistance (R) of NFC-8/2 and NFC-6/4 increased with increasing temperature from 23 °C ($R \sim 10^7 \Omega$) to 70 °C ($R \sim 10^9 \Omega$) (figure 8(D)) and from 23 °C ($R \sim 0 \Omega$) to 42 °C ($R \sim 60 M\Omega$) (figure 8(E)), respectively. Conductivity (σ) of NFCs increased with decreasing temperature from 40 °C to 27 °C (figures 9(A)–(C)). The conductivity parameters depended on the loading partner copolymer and incorporated AgNPs: $\sigma = 2.21 \times 10^{-11} \text{ S m}^{-1}$, $3.68 \times 10^{-10} \text{ S m}^{-1}$ and $2.42 \times 10^{-10} \text{ S m}^{-1}$ for NFC-8/2, NFC-6/4 and NFC-8/2-AgNPs, respectively. Activation energies (E_a) of NFCs (1.45 eV for NFC-8/2, 1.70 eV for NFC-6/4 and 0.01 eV for NFC-8/2-AgNPs) were calculated at 22 °C–35 °C temperature range from Arrhenius plots of $\ln \sigma$ versus $1/T$ using well known equation (figures 9(D)–(F)) [44]:

$$\sigma = \sigma_0 \exp(-E_a/kT),$$

where σ_0 , E_a and k are conductivity prefactor, conductivity activation energy and Boltzmann's constant ($k = 8.625 \times 10^{-20} \text{ eV K}^{-1}$), respectively. The following increase of temperature up to 65 °C had not significant effect on conductivity and activation energy.

Conductivity of NFCs also strongly depended on conduct times. Obtained results indicated that the conductivity of NFCs essentially improved with applied various conduct times from 0 min up to 4.5 h (figure 10). Maximum conductivity values of $\sigma_{dc} = 5.0 \times 10^{-8}$, 6.74×10^{-8} and $1.17 \times 10^{-6} \text{ S m}^{-1}$ were observed for NFC-8/2, NFC-6/4 and NFC-8/2-AgNPs at conduct times of 5 min, 20 min and 5 min, respectively. The kinetic plots of conductivity versus time (figures 10(D)–(F)) showed that changes in conductivity continued up to 2 h for all NFCs, and then this dependence almost stabilized up to 4.5 h. Colloidal polymer nanofibers exhibited higher conductivity when compared with those for pristine PVA ($1.25 \times 10^{-15} \text{ S cm}^{-1}$) [17] and partner copolymer ($5.0 \times 10^{-11} \text{ S cm}^{-1}$).

After the annealing process and treatment with NaOH as doping agent, the electrical resistance and conductivity of NFCs (figure 11) visible increased as compared with NFC-8/2 and NFC-6/4. Absorption of NaOH solution (0.5 M) on the samples (0.005 ml onto 0.25 cm² surface of nanofiber film with thickness $\sim 10 \mu\text{m}$) significantly increased conductivity parameters. This phenomenon observed can be explained by an increase in the ion-charged sites in the nanofiber structures via activation of carbonyl and double $-\text{CH}=\text{CH}-$ conjugation onto main chains of rearranged macromolecules. SIP around 50 °C–60 °C observed in figure 11(E) was due to transfer of nanofiber structures to glass-transition state. The presence of NaOH caused the appearance of strong second peak. It was proposed that Na^+ ions from ionized NaOH formed bridges

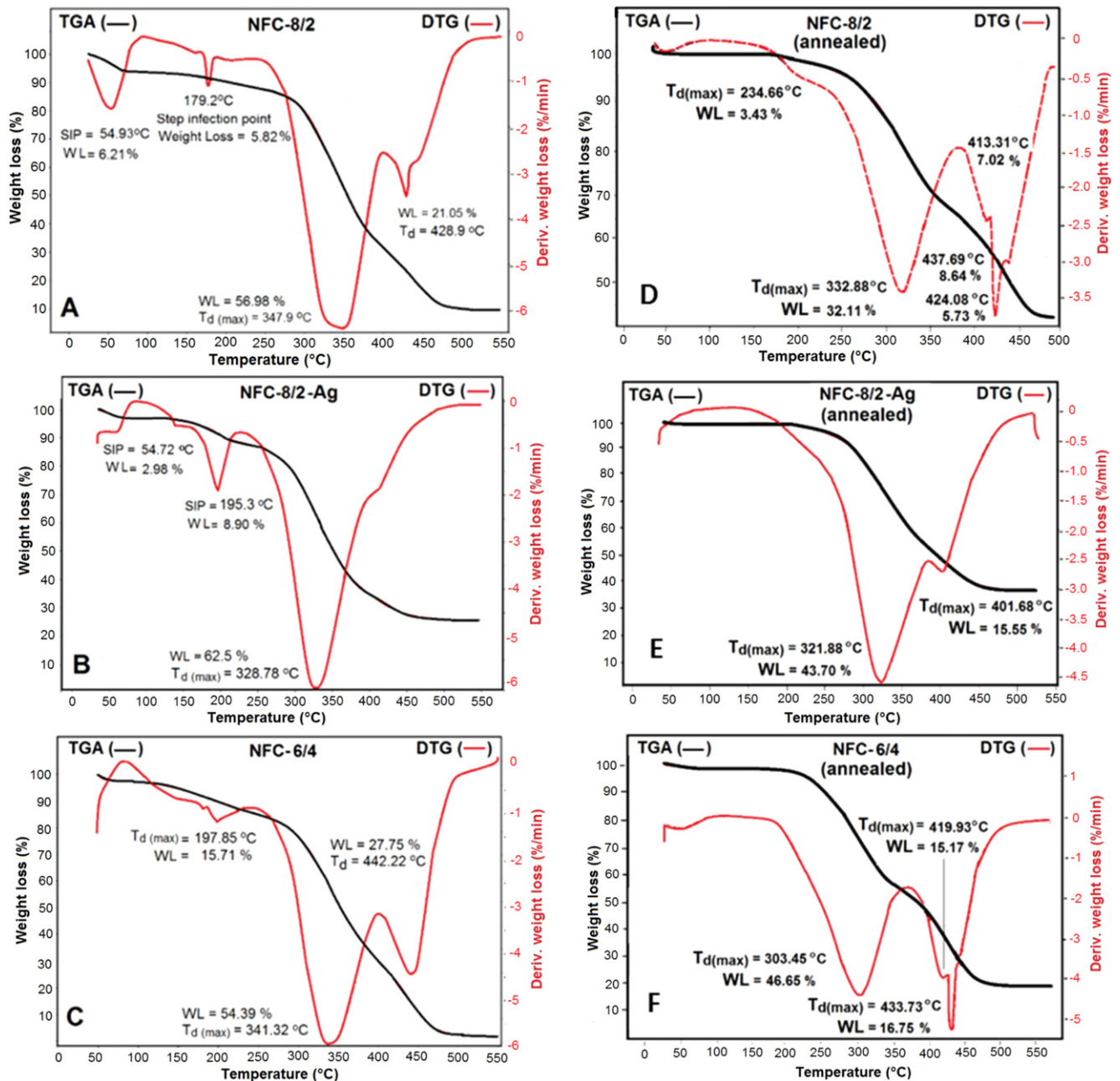


Figure 6. TGA–DTG thermograms of NFCs. (A)–(C) before and (D)–(F) after annealing.

between two $-C=O$ and $-CH=CH-$ groups onto rearranged polymer chains, and enhanced ion-charged sites, and therefore improved the conductivity of NFCs. Increase of temperature from $30\text{ }^{\circ}\text{C}$ to $70\text{ }^{\circ}\text{C}$ significantly decreased conductivity of NFC-8/2 (annealed) and NFC-8/2-annealed-NaOH (figures 11(B) and (F)). Temperature dependence of conductivity for NFC-6/4 (annealed)-NaOH predominantly decreased with an increase in the partner copolymer fraction as compared with that for NFC-8/2 (annealed)-NaOH. The conductivities of these nanofiber samples reached maximum level as $\sim 10^{-6}\text{ S m}^{-1}$ and $\sim 10^{-8}\text{ S m}^{-1}$ around $30\text{ }^{\circ}\text{C}$ – $35\text{ }^{\circ}\text{C}$. The annealing procedure and NaOH doping factors also dramatically increased conductivities of NFCs compared with those for the matrix PVA polymer.

Activation energies of NFCs without and with NaOH doping were calculated as 0.041 eV for NFC-8/2 (annealed), 1.038 eV for NFC-8/2 (annealed)-NaOH, 0.037 eV for NFC-6/4 (annealed), and 0.071 eV for NFC-6/4 (annealed)-NaOH at $30\text{ }^{\circ}\text{C}$ – $70\text{ }^{\circ}\text{C}$ temperature range. Thus, multifunctional rearranged structures and their NaOH physical modifications exhibited higher semiconductor properties.

4. Conclusions

This work presents synthesis and characterization of novel multifunctional polymer nanocomposite nanofiber electrolytes by green electrospinning nanotechnology using the

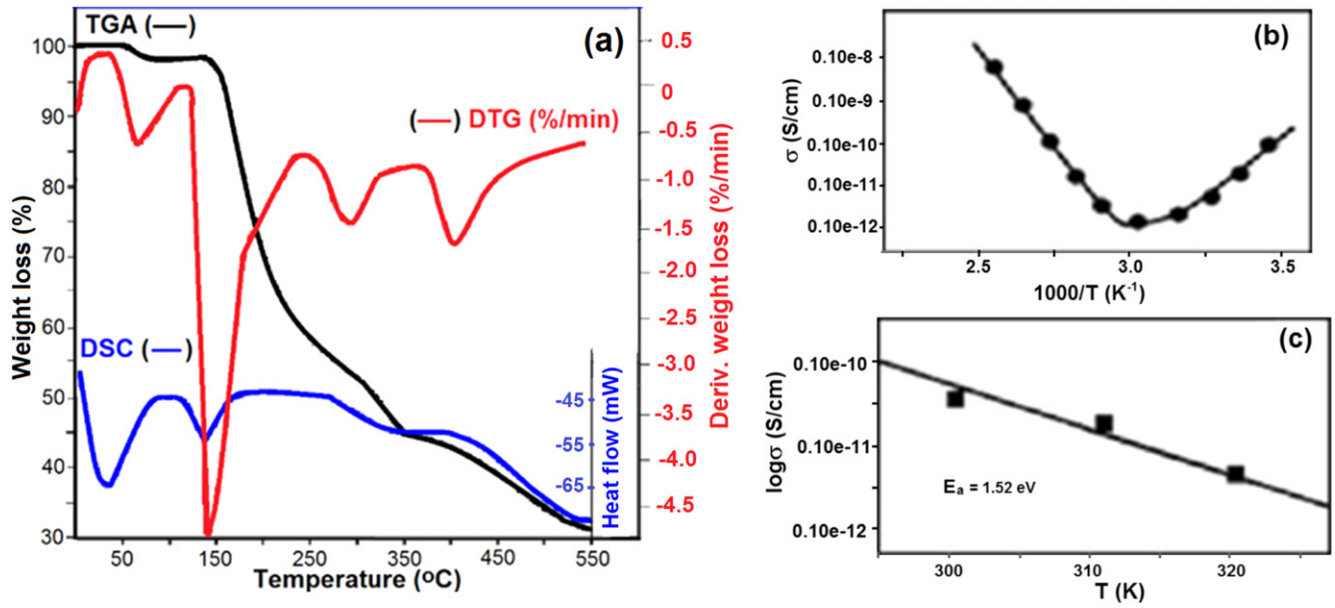


Figure 7. (a) Conductivity as a function of temperature, (b) Arrhenius plot of measured conductivity and (c) thermal behaviors of poly(MAc-alt-AA).

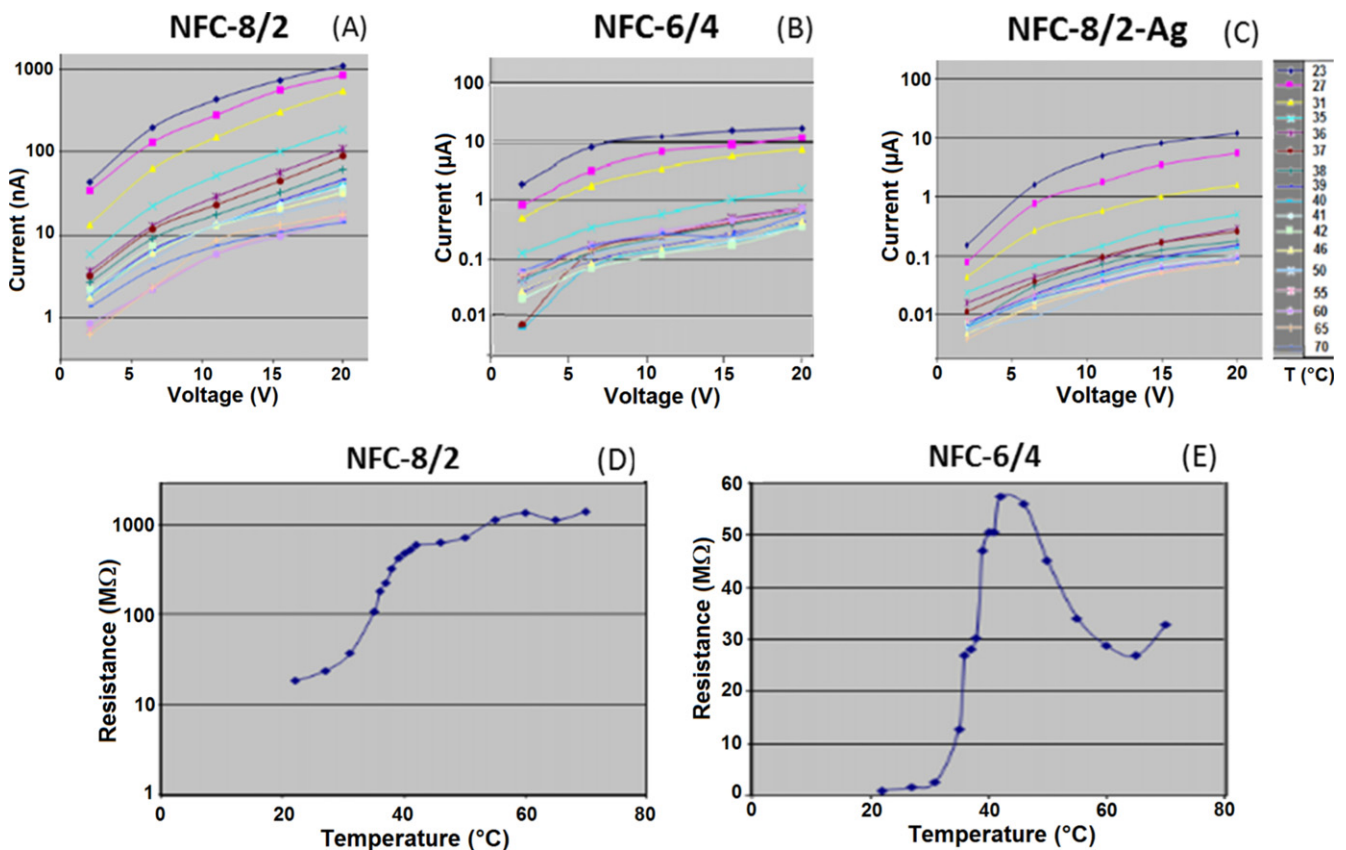


Figure 8. (A)–(C) electrical properties of NFCs and (D) and (E) temperature dependence of resistance.

water solution blends of intercalated PVA/ODA-MMT nanocomposite as a matrix polymer, poly(MAc-alt-AA) copolymer and its Ag-carrying copolymer complex as partner polymers. The crosslinked nanofibers were prepared by varying the fractions of partner copolymer enhanced with regular repeated units with carboxylate ions and AgNPs.

Chemical cross-linking of matrix PVA by reactive partner copolymer via esterification/cross-linking were observed. A covalence bridge of partner copolymer between PVA macromolecules not only reinforced the network, but also provided extra ion charged sites. The presence of the ionized and charged functional groups in the nanofiber structures as self-

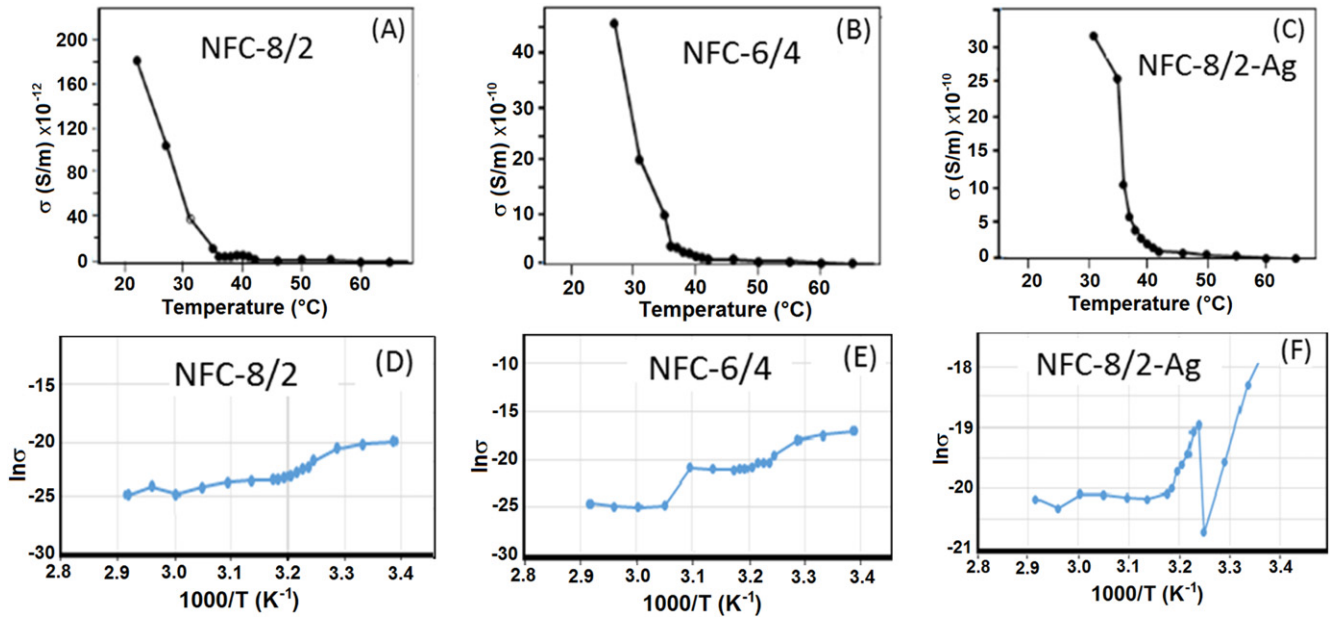


Figure 9. (A)–(C) temperature dependence of conductivity and (D)–(F) Arrhenius plots of NFCs at various temperature regions.

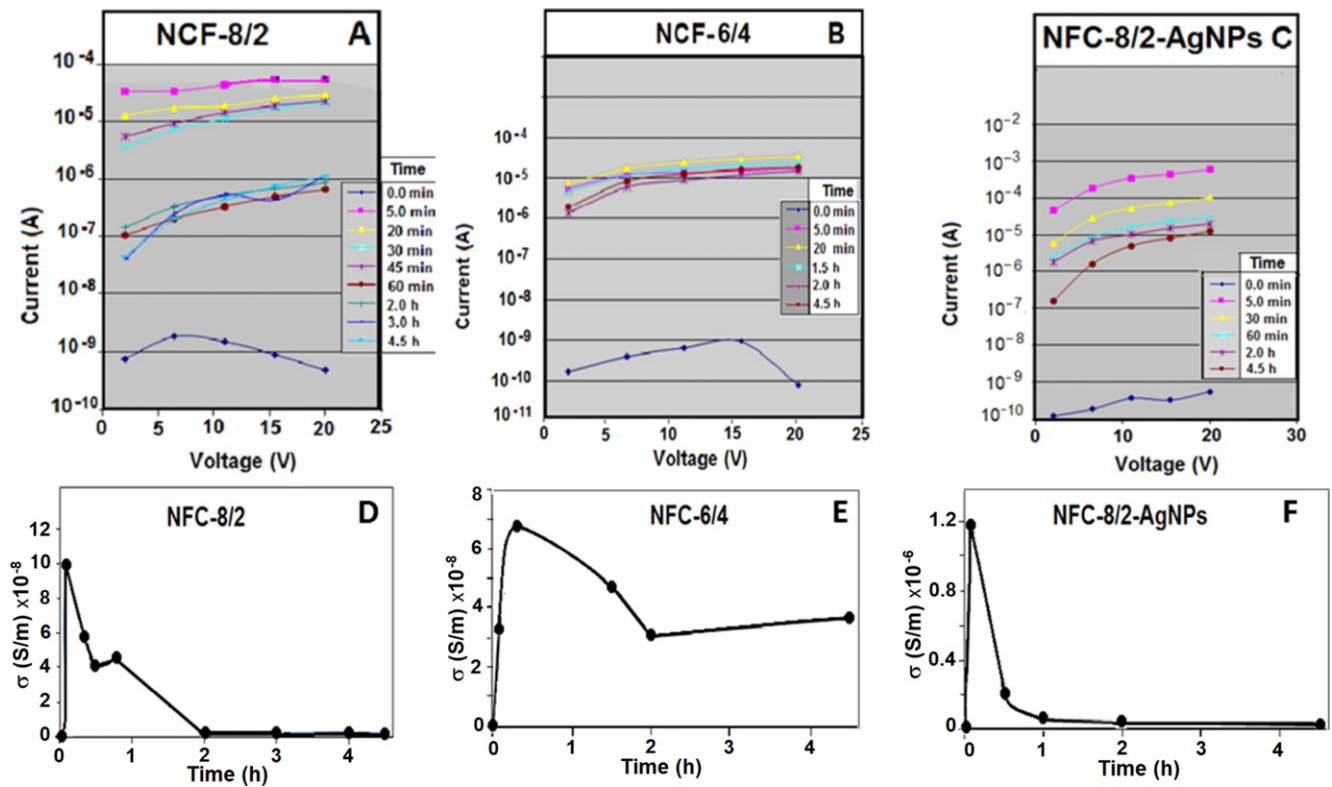


Figure 10. (A)–(C) electrical properties at various conduct time and (D)–(F) kinetic curves of conductivities for NFCs.

assembled sites were confirmed. The dominant colloidal amorphous structures which would improve their electrical properties were obtained. Nanofiber electrolytes exhibited unique morphology and diameter distributions, as well as the formation of *in situ* generated AgNPs onto fiber surfaces. Improvement in morphology and conductivity occurred due to structural rearrangement of nanofibers via decarboxylation of anhydride units of partner copolymer. This evaluated

phenomenon as an effect of structural changes can be described as new approach in polymer electrolytes. Essentially improvement of conductivity of annealed NFCs with NaOH was also estimated. The electrical parameters of NFCs also strongly depended on the fraction and alternating structure of the partner copolymer, AgNPs, applied temperature and conduct time. The obtained novel polymer colloidal nanofiber electrolytes with covalence cross-linked, rearranged and

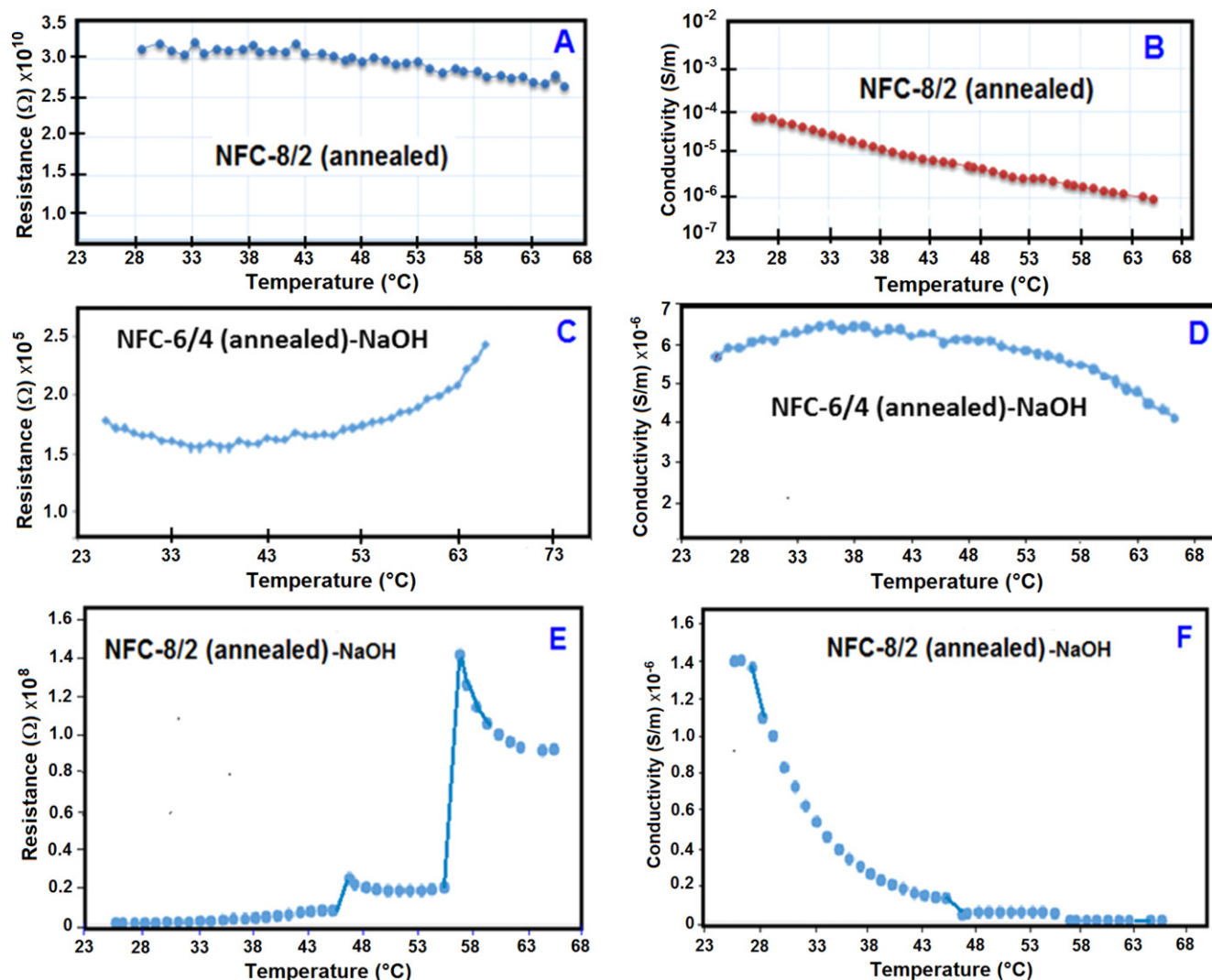


Figure 11. Relationship between electrical resistance-temperature and conductivity-temperature for NFSs. (A, B) The effect of thermally rearranged nanofiber structures and (C)–(F) NaOH doping.

NaOH doped structures can be utilized in electrochemical, nanoengineering and bioengineering processing, nanolithography, fuel cell and power nanotechnology as the reactive platforms with large contact area.

Acknowledgement

The authors thank the Turkish Scientific and Technological Research Council (TUBITAK) for the financial support of this work through postdoctoral projects TBAG–HD/249 and BIDEB-PD/2218.

References

- [1] Di Noto V, Lavina S, Giffin G A and Negro E 2011 *Electrochim. Acta.* **15** 4
- [2] Bellon-Maurel V, Calmon-Decriaud A, Chandrasekhar V, Hadjichristidis N, Mays J W, Pispas S, Pitsikalis M and Silvestre F 1998 *Adv. Polym. Sci.* **135** 139
- [3] Hallinan D T Jr and Balsara N P 2013 *Annu. Rev. Mater. Res.* **43** 503
- [4] Bloor D 1989 *Polymer Properties* vol 2 ed C Booth and C Price (Oxford: Pergamon Press) p 687
- [5] Berthier C, Gorecki W, Manier M, Armand M B, Chabagno J M and Rigaud P 1983 *Solid State Ion.* **11** 91
- [6] Wang L, Zhang L and Tian M 2012 *Polym. Adv. Technol.* **23** 652
- [7] Naebe M, Lin T, Staiger M P, Dai L and Wang X 2008 *Nanotechnology* **19** 305702
- [8] Strawhecker K E and Manias E 2000 *Chem. Mater.* **12** 2943
- [9] Nguyen T-H, Lee K-H and Lee B-T 2010 *Mater. Sci. Eng. C* **30** 944
- [10] Jung H M, Lee E M, Ji B C, Deng Y, Yun J D and Yeun J H 2007 *Colloid Polym. Sci.* **285** 705
- [11] Kim S, Hwang E-J, Jung Y, Han M and Park S-J 2008 *Colloids Surf. A* **313-314** 216
- [12] Taepaiboon P, Rundsardthong U and Supaphol P 2006 *Nanotechnology* **17** 2317

- [13] Jannesari M, Varshosaz J, Morshed M and Zamani M 2011 *Int. J. Nanomedicine* **6** 993
- [14] Galya T, Sedlarik V, Novotny I, Sedlarkova J and Saha P 2008 *J. Appl. Polym. Sci.* **110** 3178
- [15] Mahanta N, Teow Y and Valiyaveettil S 2012 *J. Nanosci. Nanotechnol.* **12** 6156
- [16] Podsiadlo P et al 2007 *Science* **318** 80
- [17] Zamri M F M A, Zein S H S, Abdullah A Z and Basir N 2011 *Int. J. Eng. Technol. IJET-IJENS* **11** 15
- [18] Rajeswarl N, Selyasekarapandian S, Karthikeyan S, Prabu M, Hirankumar G, Nithya H and Sanjeeviraja C 2011 *J. Non-Cryst. Solids* **357** 3751
- [19] Kim M J, Lee J, Jung D and Shim S E 2010 *Synth. Met.* **160** 1410
- [20] Bartholome C, Miaudet P, Derré A, Maugey M, Roubeau O, Zakri C and Poulin P 2008 *Compos. Sci. Technol.* **68** 2568
- [21] Miaudet P, Bartholome C, Derré A, Maugey M, Sigaud G, Zakri C and Poulin P 2007 *Polymer* **48** 4068
- [22] Zeng J, Hou H, Wendorff J H and Greiner A 2013 *e-Polymers* **5** 387
- [23] Park J-C, Ito T, Kim K-O, Kim K-W, Kim B-S, Khil M-S, Kim H Y and Kim I-S 2010 *Polym. J.* **42** 273
- [24] Dai W S and Barbari T A 1999 *J. Membr. Sci.* **156** 67
- [25] Kim C-K, Kim B-S, Sheikh F A, Lee U-S, Khil M-S and Kim H-Y 2007 *Macromolecules* **40** 4823
- [26] Kavlak S, Kodolbas A O, Can H K, Guner A and Rzayev Z M O 2004 *Adv. Poly. Tech.* **23** 222
- [27] Can H K, Rzayev Z M O and Guner A 2004 *J. Mol. Liq.* **111** 77
- [28] McGaugh M S and Kottle S 1967 *J. Polym. Sci. C* **5** 817
- [29] Dubinsky S, Grander G S, Shter G E and Silverstein M S 2004 *Polym. Degrad. Stab.* **86** 171
- [30] Kavlak S, Can H K, Güner A and Rzaev Z M O 2003 *J. Appl. Polym. Sci.* **90** 1708
- [31] Rzayev Z M O, Türk M and Söylemez E A 2012 *Bioorg. Med. Chem.* **20** 5053
- [32] McNeill I C, Ahmed S, Memetea L, Mohammed M N, Zaikov G E and Polishchuk A Y 1996 *Polym. Degradation Stab.* **52** 171
- [33] Martinez F, Uribe E and Olea A F 2005 *Macromol. Sci. A* **42** 1063
- [34] McNeill C 1992 *Polym. Degradation Stab.* **37** 223
- [35] McNeill I C, Ahmed S and Rendall S 1998 *Polym. Degradation Stab.* **62** 85
- [36] McNeill I C, Ahmed S and Gorman J G 1999 *Polym. Degradation Stab.* **64** 21
- [37] Świtła-Żeliazkow M 2001 *Polym. Degradation Stab.* **74** 579
- [38] Reinhardt S, Komber H and Steinert V 1996 *J. Polym. Sci. A* **34** 2415
- [39] McNeill I C, Polishchuk A Y and Zaikov G E 1995 *Polym. Degradation Stab.* **47** 319
- [40] Colthup N B, Daly L H and Wiberley S E 1990 *Introduction to Infrared and Raman Spectroscopy* 3rd edn (San Diego, CA: Academic)
- [41] Lambert J B, Shurvell H F, Berbit L, Cooks R G and Stout G H 1976 *Organic Structural Analysis* (New York: Macmillan)
- [42] Attia G and Abd El-kader M F H 2013 *Int. J. Electrochem. Sci.* **8** 5672
- [43] Li G, He D, Guan B, Gao S, Cui Y, Yokoyama K and Wang L 2012 *Int. J. Mol. Sci.* **13** 466
- [44] Rivas B L and Sequel G V 1999 *Polyhedron* **18** 2511